THE JOURNAL OF PHYSICAL CHEMISTRY C

Article

pubs.acs.org/JPCC

Molecular Insights into Carbon Nanotube Supercapacitors: Capacitance Independent of Voltage and Temperature

Guang Feng,[†] Song Li,[†] Jennifer S. Atchison,[‡] Volker Presser,[‡] and Peter T. Cummings*[,†,§]

[†]Department of Chemical and Biomolecular Engineering, Vanderbilt University, Nashville, Tennessee 37235, United States

[‡]INM—Leibniz-Institute for New Materials, Campus D2 2, D-66123 Saarbrücken, Germany

[§]Center for Nanophase Materials Sciences, Oak Ridge National Laboratory, Oak Ridge, Tennessee 37831, United States

Supporting Information

ABSTRACT: Molecular dynamics (MD) simulations of supercapacitors with single-walled carbon nanotube (SWCNT) electrodes in room-temperature ionic liquids were performed to investigate the influences of the applied electrical potential, the radius/curvature of SWCNTs, and temperature on their capacitive behavior. It is found that (1) SWCNTs-based supercapacitors exhibit a near-flat capacitance—potential curve, (2) the capacitance increases as the tube radius decreases, and (3) the capacitance depends little on the temperature. We report the first MD study showing the influence of the electrode curvature on the capacitance—potential curve and negligible dependence of temperature on capacitance of tubular electrode. The latter is in good agreement with recent experimental findings and is attributed to the similarity of the electrical double layer (EDL) microstructure with temperature varying from 260 to 400 K. The electrode curvature effect is explained by the dominance of charge overscreening and increased ion density per unit area of electrode surface.

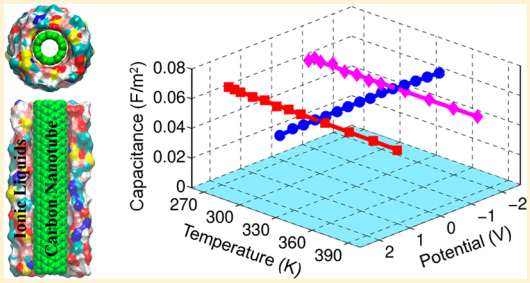

I. INTRODUCTION

Electrical double layer capacitors (EDLCs), also named supercapacitors or ultracapacitors, have attracted tremendous attention in recent years as a promising type of electric energy storage (EES) device.[1,2] This is related to their energy density which is higher than for conventional capacitors and their high power handling ability which is superior compared to batteries. To date, carbons in diverse forms such as activated carbons,[3] carbide-derived carbons,[4] carbon nanotubes (CNTs),[5,6] graphene-based composites,[7] and onion-like carbons (OLCs)[8] have been explored extensively as electrode material for supercapacitors. Among such materials, CNTs have emerged as promising candidates for fabricating high-performance supercapacitor electrodes with preeminent power handling as a result of their very high electrical conductivity and readily accessible surface area.[9,10] For instance, dielectrophoretically deposited single-walled carbon nanotubes (SWCNTs) were assembled into long ultrathin fibrils to enhance both electrical conductivity and electrochemical capacitance of carbon-based supercapacitors;[10] the densely packed SWCNTs, parallel-aligned to the direction of electrolyte ion transport, were found to serve as excellent electrodes for supercapacitors to achieve higher power density.[11]

In view of their exceptionally wide electrochemical stability window, excellent thermal stability, nonvolatility, and relatively inert nature, room-temperature ionic liquids (RTILs) have emerged as a very advanced class of electrolytes for supercapacitors.[12,13] However, the classical description of EDL formation completely breaks down for RTILs in the absence of a solvent and having a more complex molecular structure. To study RTIL-based EDLs, there is an acute need for advanced theoretical, modeling, and experimental work. To date, the most extensively studied macroscopic property of the EDLs in RTILs is the differential capacitance (δC) versus the applied potential (V).[14,15] A variety of $\delta C-V$ curves have been observed and predicted, including the U-shaped, bell-shaped, and camel-shaped ones for supercapacitors with planar electrodes.[14−18] All of these studies demonstrated that the differential capacitance significantly changes with applied cell potentials. Very recently, and in contrast to these studies, a near-flat $\delta C-V$ curve was predicted for electrodes composed of spherical OLC particles using molecular dynamics (MD) simulations.[19] However, until now, the dependency of the differential capacitance of CNT-based supercapacitors on the potential remains unknown. For this purpose, MD simulation can help greatly to derive design strategies for supercapacitor electrodes and selection criteria of the optimized size of SWCNTs. For example, it has been shown in an MD study that the capacitance of SWCNTs filled with RTILs increases with decreasing the tube diameter from 2.03 to 0.95 nm.[20] It has also been reported that few RTIL ions could enter the interior of the CNT in some experiments,[21,22] so that the electrolyte ions are electrosorbed and almost exclusively accumulated on the outer CNT surface. Theoretically, the capacitance change of the EDL exohedrally near the CNT electrode follows, on first

Received: April 10, 2013
Published: April 12, 2013

   dx.doi.org/10.1021/jp403547k | J. Phys. Chem. C 2013, 117, 9178−9186

approximation, a phenomenological scaling equation related to the tube diameter,[23] but the actual origin and mechanism underpinning this curvature effect are still unclear.

Apart from the influence of electrode curvature, it is well-known that the temperature has an important impact on the performance of supercapacitor devices. While the majority of experimental studies observed an increased capacitance with a temperature increase (positive temperature dependence),[6,24,25] some other work reported the exact opposite effect (negative temperature dependence).[16] For instance, Silva et al.[25] reported a positive temperature dependence on capacitance at the interfaces between the RTIL [bmim][PF_6] and mercury, platinum, and glassy carbon electrodes, whereas the capacitance measured at [emim][BF_4]/Hg interfaces diminishes as temperature increases from +22 to +80 °C.[16] Interestingly, most theoretical and modeling studies predict the negative temperature dependence or, at least, a complex capacitance-temperature relationship;[26−29] for example, MD simulations[27] revealed a decrease of capacitance with an increase of temperature, and Monte Carlo simulations[29] showed a bell-shaped trend delineating the dependence of capacitance on temperature. In contrast with previous observations and predictions, a recent experiment, using vertically aligned CNT electrodes and RTIL electrolytes, revealed that the capacitance was almost independent of the temperature.[21] Hence, an in-depth investigation is needed to establish a reasonable understanding of the temperature dependency as well as the fundamental mechanisms behind this interesting phenomenon.

Motivated by these considerations, in this work, we performed MD simulations to model SWCNTs-based supercapacitors with an electrolyte of RTIL 1-ethyl-3-methylimidazolium bis(trifluoromethylsulfonyl)imide ([emim][Tf_2N]). The influences of electrical potential, cylindrical electrode curvature and temperature on capacitance near different-sized SWCNT electrodes were investigated. The results reveal a unique capacitive behavior of RTIL-based supercapacitors with CNT electrodes, which originates from the special EDL microstructure and the cylindrical curvature of electrodes. The rest of this paper is organized as follows: section II describes the simulation system and methods used herein; section III includes the results on how the applied potential, electrode curvature, and operating temperature influence the capacitive behavior of CNT-based supercapacitors and the fundamental understanding of these observations; and finally, section IV presents the conclusions.

II. SIMULATION METHOD AND MODELS

As shown in Figure 1, the simulation system consists of an end-capped SWCNT immersed in a box of [emim][Tf_2N], since the experiments reported that the electrodes are made of vertically aligned CNT arrays with large intertube distance for ion accessibility and the EDLs in RTILs form exclusively on the outer surfaces of CNTs.[21,22] The length of SWCNT with caps is about 8.0 nm (cap height is ∼0.3 nm), and the tube radius, R, ranges from 0.41 to 1.01 nm. The simulation temperature varies from 260 to 400 K, since the melting point of [emim][Tf_2N] is below −17 °C as reported experimentally.[30,31] The upper limit (400 K) is far beyond the limit of conventional supercapacitors and was chosen as a practical application cutoff.

MD simulations were performed in the canonical ensemble using a user-modified version of MD package GROMACS.[32] Periodic boundary conditions were used in three dimensions, and the simulation was run in the isothermal−isobaric ensemble, which tuned the box size automatically. The force fields for the electrode atoms (carbon) and ions in [emim]-[Tf_2N] were the modified Atomistic Polarizable Potential for Liquids, Electrolytes and Polymers (APPLE&P).[33,34] The only modification applied herein is excluding the polarizability terms from APPLE&P force field for the sake of efficient simulations. It is worthwhile to note that neglect of polarizability displayed slight influence on the structural properties and relatively significant effects on the dynamics properties; despite this, the nonpolarizable APPLE&P force fields are still more reasonable compared with other predictions reported in the literature using nonpolarizable MD models.[34]

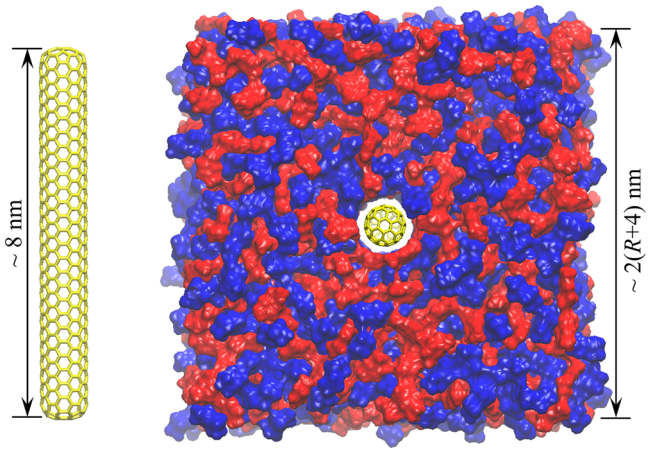

Figure 1. Snapshot of the MD simulation system. The single-walled carbon naonotube with radius R is in yellow on the left. Red and blue spheres denote [emim]$^+$ and [Tf_2N]$^-$ ions, respectively. Some molecules of ionic liquids were removed to display the capped SWCNT.

To generate the potential between electrode surface and the bulk electrolyte (about 4 nm far from the electrode surface), the partial charges were uniformly distributed among the electrode atoms. Particularly, to weaken the edge effects from the caps of SWCNT, no charge was assigned to atoms on the caps. In order to make the neutrality of the system, when the SWCNT electrode carries integral charges in units of e, the numbers of RTIL cations and anions are adjusted to have the same amount of charges in total but with the opposite sign. For example, a simulation consists of a SWCNT with total charges of 8e- and a box of ILs having 828 [emim]$^+$ and 820 [Tf_2N]$^-$.

The number and charge density profiles of EDLs were computed along the radial direction from the SWCNT surface to the RTIL bulk, excluding the ∼2 nm-long end of the SWCNT, based on our previous study.[35] To examine whether this method works well for ruling out the end/edge effects, additional simulations in the NVT ensemble were performed using a SWCNT periodically along its axis direction (same as the simulation setup in ref 36). The number and charge density profiles as well as the capacitance obtained from two different sets of simulations were found to be almost the same.

Additionally, simulations of EDLs in [emim][Tf_2N] near a single graphene sheet with open surface under different applied potentials were performed to provide a baseline for comparison. Each MD simulation system consisted of a slab of electrolytes enclosed inside a channel with two electrodes,[36−38] and each electrode was modeled as a single graphene sheet with an area of 4.26 × 4.18 nm^2, compared with a single-walled CNT. To generate the different applied potentials, the

dx.doi.org/10.1021/jp403547k | J. Phys. Chem. C 2013, 117, 9178−9186

partial charge was uniformly distributed among the carbon atoms of two planar electrodes. To make the neutrality of the channel system, two single graphene sheets carry the same surface charge with opposite sign. The gap between the opposing electrode surfaces was chosen as 7.0 nm and the number of ion pairs was tuned until the electrolytes in the central portion of the system have the same density as that in the simulation of bulk ILs. In addition, note that in this work, (1) the cylindrical or planar electrode consists of single-walled CNT or single graphene sheet, which is different from the electrodes comprised of multiple layers of the onion-like carbons or graphene sheets in ref 19; (2) the image charge effect stemming from the electrode is neglected, and then the partial charges are placed on the carbon atoms of the electrode rather than on an image plane used in ref 19 (image plane was set as a plane 0.07 nm away from the geometrical plane of each graphene surface). These two differences do affect the magnitude of EDL capacitance but do not change the relationship between capacitance and potential as well as electrode curvatures, which are validated by simulations with and without these two different settings. The potential distribution profile across the EDL was computed based on the space charge density obtained from MD simulations, and the detail can be found in the Supporting Information (SI).

In the simulation systems (for both cylindrical and planar electrodes), the electrolyte temperature was maintained at a setting value using the Berendsen thermostat. The electrostatic interactions were computed using the PME method.[39] Specifically, an FFT grid spacing of 0.10 nm and cubic interpolation for charge distribution were used to compute the electrostatic interactions in reciprocal space. A cutoff distance of 1.1 nm was used in the calculation of electrostatic interactions in the real space. The nonelectrostatic interactions were computed by direct summation with a cutoff length of 1.1 nm. The LINCS algorithm[40] was used to maintain the bond lengths within the $[emim]^+$ cation and $[Tf_2N]^-$ anion. Each simulation was started at 1000 K and subsequently annealed gradually to a certain temperature in 6 ns. Following annealing, the system was simulated at that temperature for another 6 ns to reach equilibrium. A 9 ns production run was performed after equilibration and used for result analysis as shown in the following section.

III. RESULTS AND DISCUSSION

Differential Capacitance. The $\delta C-V$ curves for different-sized SWCNT-based supercapacitors at 333 K were investigated first. The differential capacitance was computed as $\delta C = d\sigma/dV_{EDL}$. Here, σ is the surface charge density on the electrode surface and V_{EDL} is the potential applied on EDLs such that $V_{EDL} = \phi_{EDL} - PZC$, where ϕ_{EDL} is the potential difference between the electrode surface and the bulk electrolyte and PZC is the potential of zero charge (see also the SI). The differential capacitance for EDLs near SWCNTs with different radii and, for comparison, a planar graphene sheet is displayed in Figure 2. We observe that the capacitance of CNTs is higher than the planar electrode. The capacitance magnitude (~0.04−0.06 F/m^2) is close to that reported by simulations with the similar RTILs near planar carbon electrodes.[27,41] Moreover, the $\delta C-V$ curves are almost flat for CNT electrodes, whereas the $\delta C-V$ curve near planar electrodes is pronouncedly bell-shaped which is in perfect agreement with previous studies;[19,42] the differential capacitance of SWCNT electrodes is nearly independent of the applied potential regardless of the CNT radius changing from 0.41 to 1.01 nm. Specifically, the mean value of the $\delta C-V$ curve is 0.051 ± 0.001 F/m^2 for the SWCNT radius of 1.01 nm (the largest CNT explored here), and the overall line shape is very different from the U-shaped, bell-shaped, camel-shaped, or other complex shaped $\delta C-V$ curves reported in literature.[14−18,43] Also, the distinct behavior of the near-flat $\delta C-V$ curve becomes more pronounced when the SWCNT radius is reduced: as CNT radius reduces from 1.01 to 0.41 nm, the deviation of the $\delta C-V$ curve to its mean value varies from 2.6% to 1.3%. In other words, this demonstrates the very small potential dependency of the differential capacitance and there is even less of a variation of the differential capacitance when the tube curvature is increased (Figure 2).

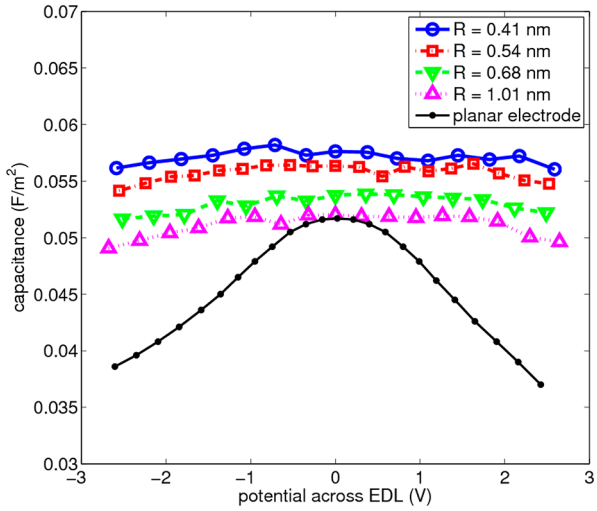

Figure 2. Differential capacitance as a function of the applied potential on SWCNTs-based supercapacitors. R is the tube radius. For comparison, data (black line with dot markers) are also shown for planar electrodes modeled by flat single graphene sheet.

Traditionally, the bell-shaped $\delta C-V$ curve of EDLs near the planar electrode is attributed to the charge overscreening at small/moderate voltages and evolving lattice saturation at large voltages.[42,44] Conceptually, the charge overscreening describes the phenomenon that the counter-charge from ions adsorbed on the electrode exceeds the electron charge on the electrode (i.e., the charged electrode is overscreened); for highly charged surfaces, when all counterions needed to counterbalance the charge on the electrode cannot be packed in the nearest single layer of the electrode, several consecutive layers of counterions would accumulate on the electrode, and then lattice saturation occurs.[14,42,44,45] Specifically, the charge overscreening has been demonstrated as a universal feature of EDLs due to the high ionic density and strong ion coupling in RTILs, which dominates the EDL capacitance at the planar and spherical electrodes under small/moderate voltages.[19] Thus, we explored the origin of the near-flat $\delta C-V$ curve by investigating charge overscreening at the interfaces of RTILs and cylindrical electrodes. For that, we introduce a charge-screening factor to quantify the screening efficiency along an EDL, according to eq 1:

$$C_f(u) = -\frac{1}{\sigma}\int_{u_0}^{u}\left(\frac{s}{R}\right)^N \Delta\rho_e(s)\,ds \qquad (1)$$

where u_0 is the location of electrode surface (in this study, u_0 = 0 is for planar electrode and $u_0 = R$ is the radius of the outer

dx.doi.org/10.1021/jp403547k | J. Phys. Chem. C 2013, 117, 9178−9186

electrode surface, for SWCNTs); N = 0 is for the planar electrode, and N = 1 and 2 are for cylindrical and spherical electrodes, respectively; $\Delta\rho_e$ is the variation of space charge density as the surface charge density changes from 0 to σ (see also Figure S1 in the SI for the space charge density profile). Finally, we note that values of $C_f > 1.0$ indicate the occurrence of charge overscreening.

The charge-screening factors across EDLs near the planar graphene and a SWCNT with radius of 1.01 nm are shown in Figure 3, panels a and b, respectively. The height of the first

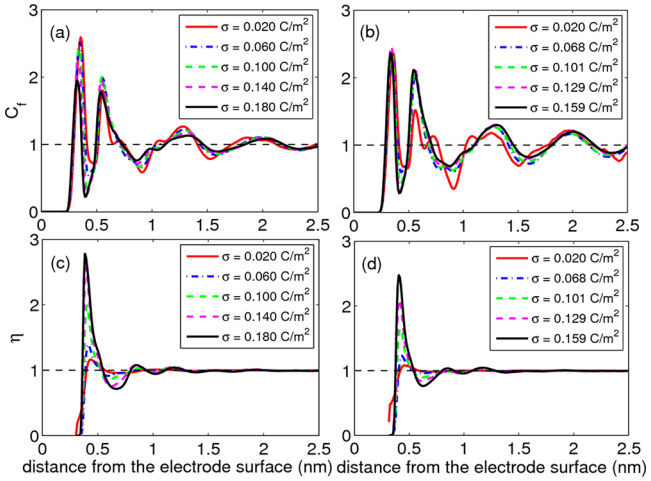

Figure 3. Charge-screening factor (C_f) across EDLs in the RTIL [emim][Tf_2N] near planar electrodes (a) and cylindrical electrodes with radius of 1.01 nm (b) and the packing factor (η) across EDLs near planar electrodes (c) and cylindrical electrodes with radius of 1.01 nm (d) at varying surface charge densities (i.e., different applied potentials).

peak of the charge-screening factor was taken as the overscreening factor, β, to quantify the charge overscreening of the EDL. It is observed that, as the electrode becomes more charged, the charge overscreening decreases for planar electrodes but changes very little for cylindrical electrodes throughout the $\delta C-V$ curves. In detail, the overscreening factor reduces from 2.62 to 1.93 for planar electrodes, whereas a SWCNT with radius of 1.01 nm has $\beta = 2.43 \pm 0.08$ for all studied charge densities, and similar small variations were found for all other SWCNTs explored in this study. Thus, the change of charge overscreening accounts for the trend of $\delta C-V$ curves near different electrodes. That is, within the working voltage range studied here, the planar electrodes in RTILs experienced a potential dependent decay in the charge overscreening which resulted in the bell shaped $\delta C-V$ curve; the highly curved surface of the SWCNT electrode material realized nearly constant overscreening that was nearly independent of applied potential, leading to a near-flat $\delta C-V$ curve.[19]

However, from the concepts of charge-screening enhancement and lattice saturation used to explain for the $\delta C-V$ curves,[14,42,44,45] it is still unclear whether the overall $\delta C-V$ curves for SWCNT and planar graphene electrodes are dominated by the charge overscreening alone or by both charge overscreening and lattice saturation. To scrutinize the existence of lattice saturation, we introduce a packing factor defined as the ratio between ions within a certain distance from the charged electrode and those from the neutral electrode according to eq 2:

$$\eta(u) = \int_{u_0}^{u} s^N \rho_n^{\sigma}(s)\, \mathrm{d}s \Big/ \int_{u_0}^{u} s^N \rho_n^{\sigma=0}(s)\, \mathrm{d}s \qquad (2)$$

u_0 and N are same as defined in eq 1, and ρ_n^{σ} is the number density of an EDL with a surface charge density of σ. The packing factor across EDLs near planar and cylindrical electrodes is displayed in Figure 3, panels c and d, respectively. It is observed that the maximum packing factor is located at the same position, about 0.4 nm, as that for the first peak of counterion density profile in the EDL (Figure S2). The maximum packing factor was exhibited as a function of electrode surface charge in Figure S3, which shows that the peak intensity becomes larger as the electrodes, both planar and cylindrical, carry more charges. This clearly suggests that more ions can be accumulated into the first layer of the EDL, because there is still some empty space for ions to come in contact with the electrode surface. Thus, lattice saturation is not observed within the potential range (−2.6 to +2.6 V) studied in Figure 2, although it has been predicted to occur at larger voltages.[42,44] This effect could arise from the relatively small size of $[emim]^+$ and $[Tf_2N]^-$ ions,[46] whereas larger RTIL ions would eventually cause lattice saturation at even moderate voltages.

It is important to note that the potential window studied here (i.e., 5.2 V) actually corresponds to twice the potential observed in symmetric 2-electrode devices used in commercial applications. Considering the operating voltage of most RTILs lies below 5 V (e.g., 3.5 V for [emim][Tf_2N]),[47] there would be no lattice saturation found experimentally during the charging/discharging process of RTIL-based supercapacitors with planar, cylindrical, or spherical electrodes when the RTILs have the similar size and shape with the [emim][Tf_2N] molecules. The absence of ion saturation was even observed in a 0.78 nm carbon pore filled with similar imidazolium-based RTILs under an applied potential greater than 5.5 V.[48] It is, however, difficult to extrapolate our findings to other, much more complex and significantly larger RTIL molecules.

With further examination of Figure 3, panels c and d, we observe that the packing factor actually approaches unity no more than around 1.1 nm from the charged electrode surface. In detail, the threshold value is about 1.1 nm for planar graphene and 0.82 nm for SWCNTs, and beyond that value, the packing factor remains almost constant with slight oscillations of ±4%. Although this indicates that the EDL mainly contributing to energy storage is no more than 1.1 nm in thickness, we also note that the majority of research studies have reported that the layering of cations and anions in RTILs near the electrode surface is about 1.5−3.0 nm in thickness.[27,38,41,43,49] Essentially, due to the strong cation−anion interaction and ion adsorption on the electrode, the EDL is composed of alternating cation/anion layers, even near the neutral electrode. Hence, the microstructure of EDLs in RTILs near charged electrodes becomes more complicated and difficult to be fully understood, since the original complexity occurring at neutral electrodes hides the nature of the layers for energy storage. Thus, it follows that although the distinct EDL layering structure could penetrate into the bulk ILs about 1.5−3.0 nm, the EDL within the first ∼1.1 nm from the electrode surface (or no more than first two peaks in an EDL) is majorly responsible for the energy storage, and beyond that region, the electrolyte can be considered as a "generalized solvent" that contributes little to the energy storage.[37]

Curvature Influence on Capacitance. In this study, the curvature is defined consistently as the reciprocal of SWCNT

dx.doi.org/10.1021/jp403547k | J. Phys. Chem. C 2013, 117, 9178−9186

radius (i.e., $1/R$). The integral capacitance was computed by $C = \sigma/V_{EDL}$ at an applied potential of 1.4 V for a one-electrode setup, which corresponds to 2.8 V experimentally used in symmetrical CNT-based supercapacitor devices.[21] Note that the following analysis of capacitance will be at the fixed potential of 1.4 V, since the contribution to the capacitance is nearly identical for the cathode and anode due to the similar size of $[emim]^+$ and $[Tf_2N]^-$ ions.[46] It can be seen from Figure 4 that the capacitance increases as the tube radius decreases.

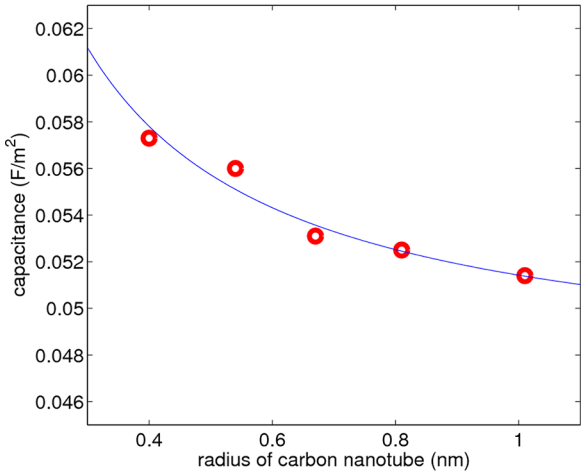

Figure 4. Integral EDL capacitance as a function of the SWCNT radius under a potential of 1.4 V. The red circles denote the MD data, and the blue line indicates the fitting curve using eq 3.

The capacitance-radius relation for the EDL at the outer surface of the cylindrical electrode can be described by a phenomenological scaling equation in form of eq 3[23]

$$C = \frac{\varepsilon_r \varepsilon_0}{R \ln(1 + d_{EDL}/R)} \quad (3)$$

where ε_r is the dielectric constant of the EDL and d_{EDL} is the effective thickness of an EDL near a cylindrical electrode. Fitting eq 3 to the simulation results (Figure 4) computes ε_r = 1.47, which is reasonably larger than the vacuum value of 1. We also obtain d_{EDL} = 0.29 nm, which is in line with the effective thickness (~0.27 nm) from the "counter-charge layer in generalized solvents" (CGS) model[37] describing the EDLs in a RTIL [bmim][BF_4]. Note that d_{EDL} is a fitting value obtained implicitly from eq 3, rather than the EDL thickness measured explicitly in simulation or experiment. Assuming the curvature be close to zero, eq 3 could be reduced to $C = \varepsilon_r\varepsilon_0/d_{EDL}$ which is the common model for a capacitor with planar electrodes.[23] Using fitting parameters, calculated above, of ε_r and d_{EDL}, the EDL capacitance near planar electrodes under the same potential of 1.4 V can be computed as 0.045 F/m^2, which is close to the value obtained from MD simulation (~0.047 F/m^2).

The capacitance increasing with curvature in Figure 4 can be attributed to the enhanced ion packing on the electrode under a same applied potential.[19] That is, more ions can be accumulated over the same electrode surface area as the cylindrical curvature increases. Ion accumulation can be quantified by counting the number of ions in a layer (called layer I) over the unit area of electrode surface. Based on the microstructure of EDLs in Figure 3 and Figure S2, layer I was chosen to be within 0.00−0.82 nm of all CNT electrodes studied. This agrees with the conclusion drawn by previous computational studies that, when the absolute value of the charge density is beyond around 0.03−0.05 C/m^2, the counterions dominate the microstructure of the EDLs up to ~1.0 nm near the electrode.[27,38,41,50] Figure S4 exhibits the number of counterions within layer I as a function of the SWCNT radius. We can clearly see that at 1.4 V, for the same area of the electrode surface, more counterions are accumulated in layer I as the SWCNT radius decreases. As a result, the capacitance normalized to the electrode surface area increases with curvature. Recent MD simulation studies have illustrated the influence of surface topography on the EDL structure and capacitance.[41,50] It was found that the capacitance of EDLs at the atomically corrugated prismatic face of graphite was around 25% larger than that at the atomically flat basal plane of graphite using the same RTIL electrolyte. Considering that the atomic scale corrugation was quite similar to the cylindrically curved surface, the capacitance increase could be attributed to the curvature increase depicted in eq 3.

Temperature Influence on Capacitance. To investigate the influence of the temperature on the EDL capacitance, a series of MD simulations were performed for supercapacitors with the same RTIL and SWCNT as before but at varying temperatures from 260 to 400 K. A SWCNT with a radius of 0.41 nm was taken as the electrode, carrying a surface charge density of σ = 0.101 C/m^2. The EDL capacitance was computed and exhibited as a function of temperature, shown in Figure 5a. Deviating from a mean value only by ±2.5%, the

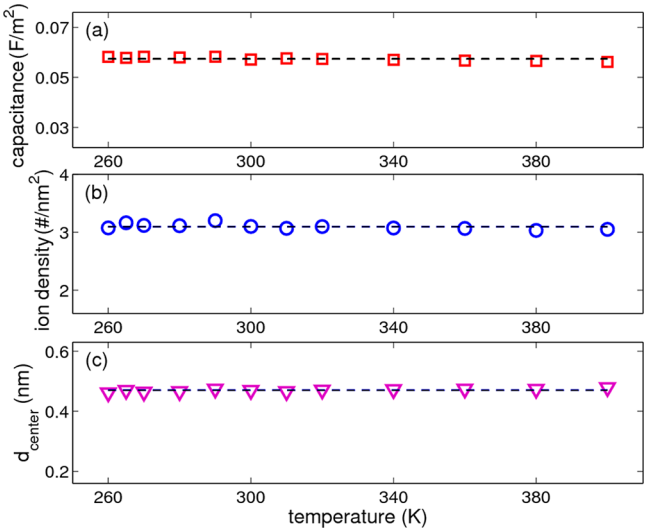

Figure 5. Capacitance of EDL (a), the accumulation of counterions (b), and the center location of counterion layer (c) near the outer surface of a SWCNT with a radius of 0.41 nm as a function of the temperature. The black dash line represents the mean value of the data points in each panel.

capacitance was found to be almost independent of temperature. The same temperature-capacitance relation was observed at the negatively charged SWCNT electrode, shown in Figure S5. This relation is in agreement with the very recent experimental finding reported by Lin et al. using a mixture of structurally related neat RTILs and CNT electrodes.[21] Note that entanglement of CNTs normally occurs in CNT electrode and makes the outer CNT surfaces not fully exposed to bulk electrolytes, so that the temperature may have different impacts

dx.doi.org/10.1021/jp403547k | J. Phys. Chem. C 2013, 117, 9178−9186

on the specific capacitance. For example, Masarapu et al. observed that the capacitance increased with temperature in experiment of a coin cell supercapacitor assembled with free-standing SWCNT film electrodes with using 1 M [TEA][BF_4] in propylene carbonate as the electrolyte.[6] This positive temperature dependence probably could be ascribed to the complex entanglement of the long SWNT strands or weakening of the ion solvation shell that are rare or absent in supercapacitors with vertically aligned CNT electrodes and RTIL electrolytes.[6,21] However, it is clear that a more detailed study of the capacitance-temperature dependency is required to fully establish a comprehensive understanding of this important aspect for the application of supercapacitor devices.

To rationalize the temperature influence on the capacitance, a Monte Carlo study of the capacitance of the double layer near a charged wall suggested that a change in ion packing, especially, the location of counterions from the charged surface is the key to determine the capacitance trend as the temperature varies.[28] Here, we first evaluated the amount of ions accumulated on the CNT electrode at temperatures ranging from 260 to 400 K. The number of counterions in layer I (0.00−0.82 nm), representing the counterion accumulation ability, is shown as a function of temperature in Figure 5b. Second, to quantify the location of layer I with respect to the electrode surface, the distance, d_{center}, is introduced in the following form shown in eq 4 similar with our previous work[51]

$$d_{center} = \int_{u_0}^{layerI} s^N(s - u_0)\rho_n(s)\,ds \Big/ \int_{u_0}^{layerI} s^N\rho_n(s)\,ds \quad (4)$$

and it is the separation between the electrode surface and the location of the center of the counterion layer. Figure 5c shows how d_{center} changes with the temperature. In short, it can be seen d_{center} as well as the ion accumulation is largely insensitive to temperature, which leads to the invariance of capacitance. Based on this analysis, the negative temperature dependence on capacitance, revealed by Vatamanu et al.[27] in an MD computational study on the interfaces of RTILs and planar graphene electrodes, could arise from the variation of ion accumulation and layer location as temperature changes.

To gain fundamental insights into the correlation between the temperature and EDL structure as well as capacitance, Holovko et al.[26] introduced a concept of ionic association; it was suggested that an increase of capacitance at higher temperatures was ascribed to a dramatic decrease in ion-pair association. This decreased ion coupling due to temperature increase was invoked to explain the positive temperature influence disclosed in many experiments.[15,24,52] In our investigation, we first addressed how to interpret the nearly flat capacitance-temperature relation observed in Figure 5a in terms of the ionic association.

From the MD simulations,[32] we can calculate the interaction potential on an ion. This potential has two parts: ion−electrode and ion−ion interactions; each part can be specified by two components: (1) the nonelectrostatic interaction rooted in van der Waals forces between the ion−electrode or ion−ion, and (2) the electrostatic interaction stemming from the charges distributed on the electrode or ions. To explore the temperature effect on ion association, we computed the interaction potential between $[Tf_2N]^-$ anions (as the counterions) and $[emim]^+$ cations across the EDL near the same positively charged electrode under varying temperatures. Specifically, the van der Waals and electrostatic interaction potentials between anions and cations were compared in Figure 6, panels a and b. We observe that the potential for anion−cation interaction becomes less negative at higher temperature, suggesting that the ionic association does, indeed, decrease as the temperature increases, which is consistent with previous computational observations.[26] Figure 6a and Figure 6b also indicate that (1) the electrostatic interactions between ions led to the ionic dissociation and (2) the confinement from electrode surface weakened the ionic association.

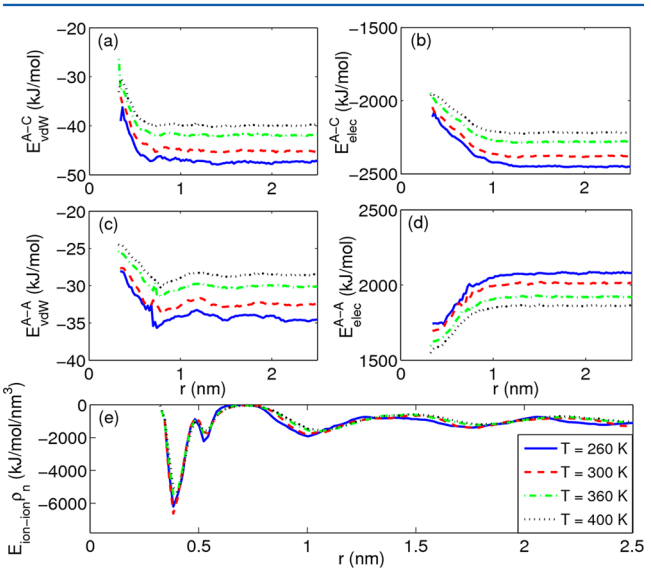

Figure 6. Interaction potential between ions in EDLs as a function of distance from electrode under different temperatures: (a) anion−cation van der Waals interaction (E^{A-C}_{vdW}), (b) anion−cation electrostatic interaction (E^{A-C}_{elec}), (c) anion−anion van der Waals interaction (E^{A-A}_{vdW}), (d) anion−anion electrostatic interaction (E^{A-A}_{elec}), and (e) the total interactions between anions per volume and other ions ($E_{ion-ion}\rho_n$). All electrodes have the same radius of 0.41 nm and carry the same surface charge density of 0.101 C/m^2.

However, if that is so, then, why did the weakened ion pairs not result in an enlarged capacitance as the temperature increases? In order to answer this question, we computed the interaction potential between anions under different temperatures (Figure 6, panels c and d). Although the anion−anion van der Waals interaction potential tends to be less negative as the temperature increases, the anion−anion electrostatic interaction potential becomes much less positive, which counterbalances the changes due to anion−cation interactions. Such compensation effects can be further confirmed by the product of the total potentials and the number density of anions across the EDLs (i.e., the resulting potential on anions per volume), as shown in Figure 6e. Taking into account the same anion-electrode interaction potentials due to the very similarly charged and same sized electrode, the overall potential on anions changes only marginally as a function of the temperature, leading to the similar ion distribution as well as the near-constant capacitance. However, we also note that from these (equilibrium) energy considerations, we cannot make assumptions on the power handling ability of such SWCNTs-based supercapacitors, (i.e., how fast the system can be charged and discharged). Generally, it is largely related to ion mobility and the constitution of the electrode.

dx.doi.org/10.1021/jp403547k | J. Phys. Chem. C 2013, 117, 9178−9186

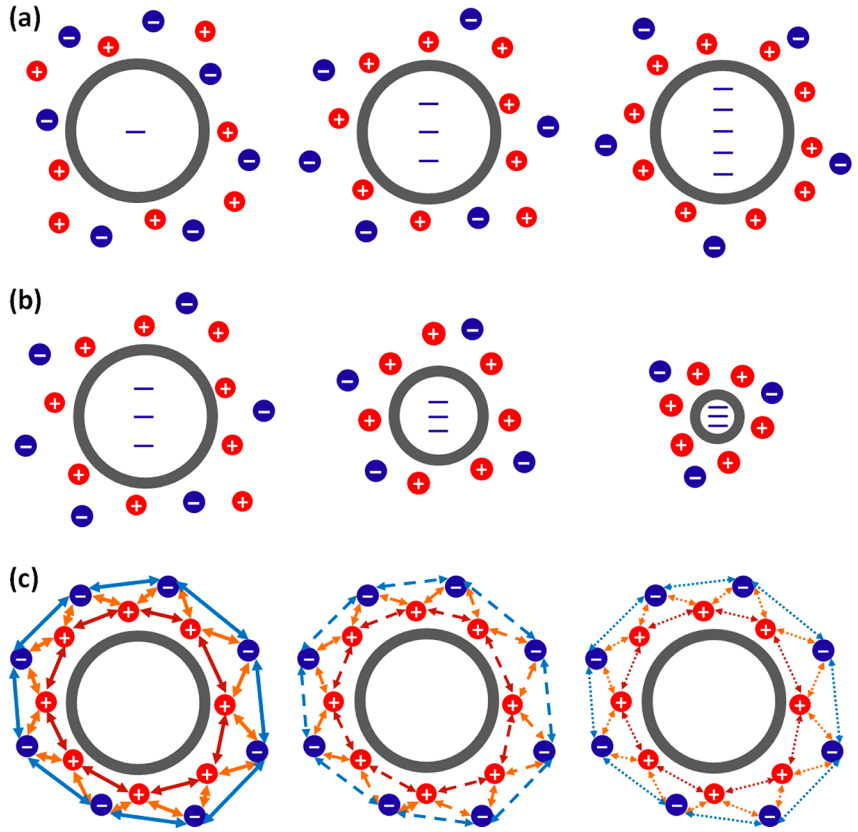

Figure 7. Schematics of fundamental insights into the influences of electrode surface charge (a), electrode curvature (b), and temperature (c) on capacitance of CNT-based supercapacitors. The red solid circles with "+" denote the cations; the blue with "−" for anions; the dark annuli represent the SWCNT; the double-arrow lines represent the interactions between ions (the lines change from the solid to the dash and then the dot with thinner line width, representing the weaker interactions). The surface charge, tube curvature, and temperature increase from the left to the right.

IV. CONCLUSION

We investigated the influences of the applied potential, electrode curvature, and temperature on the capacitance of SWCNT-based supercapacitor electrodes with a RTIL [emim]-[Tf_2N] as electrolyte using MD simulations. For the first time, a near-flat capacitance−potential ($\delta C-V$) curve was reported for EDLs near tubular carbon nanoparticles. This is in contrast with the U-shaped, bell-shaped, or the camel-shaped curve observed in RTILs on planar electrodes.[14−18,43] Within the voltage range studied here, the charge overscreening accounts for not only the almost flat $\delta C-V$ curve near the CNT electrode but also the bell-shaped curve near planar graphene electrode. The examination of the ion packing across EDLs reveals that (1) although the lattice saturation was predicted under large voltage[42,44] it would not be found at the interfaces between carbon electrode and RTILs with similar size to [emim][Tf_2N] and (2) the EDL within about 1.1 nm from the electrode contributes the most part of the total energy storage, though the fine structure of the cations and anions layering was observed to extend up to 3.0 nm into the bulk electrolyte.[27,38,41,43,49] These observations along with the understanding are schematized in Figure 7a, which shows that, due to the curvature effects originating from the CNT electrode, the overbalanced counter-charges increase proportionally to the surface charge as the electrode surface gets more charged, and the changes of ion packing mainly take place in the first two layers of ions. Moreover, the capacitance of EDL under the same potential was found to increase with the curvature of electrode surface, which is ascribed to the increased ion accumulation ability as the SWCNT radius reduces (Figure 7b). This provides a facile method to achieve an enhanced energy density for supercapacitor developed with electrodes based on highly curved materials.

The capacitance of EDL near the CNT electrode is observed to be nearly independent of the temperature, at least within the range between 260 and 400 K, which computationally reproduces the novel experimental findings by Lin et al.[21] for the first time. The subtle change of EDL structure, characterized by the ion accumulative ability and layer center location, accounts for this temperature influence on capacitance. Although the ionic association (i.e., the interactions between cations and anions) weakens as the temperature increases, the interactions among ions of the same sort also become weaker, which corporately results in the similar ion packing as well as the capacitance (Figure 7c).

The unique capacitive behavior of SWCNT-based supercapacitors, that is, the nearly flat $\delta C-V$ curve and the temperature-independent capacitance revealed in MD simulations herein, invites further experimental explorations to take advantage of these phenomena and will benefit the future design and improvement of supercapacitors with stable capacitive performance. In particular, the prospect of using RTIL-based supercapacitors which provide safe and reliable operation within a very large temperature window from below the freezing point of water to beyond the boiling point of organic solvents is of paramount interest to commercial applications.[13,21] However, we note that from the temperature independence of capacitance, we cannot predict the actual

dx.doi.org/10.1021/jp403547k | J. Phys. Chem. C 2013, 117, 9178−9186

device performance regarding the power rating and charge/discharge rates which greatly depend on ion mobility rather than ion packing. In addition, this unique capacitive behavior revealed in this study also raises the interesting question of whether a similar capacitive observation can be found for CNT-based supercapacitors using other electrolytes (e.g., different RTILs or solvent electrolytes).

■ ASSOCIATED CONTENT

Supporting Information

Details of the calculation of potential distribution and the microstructures of electrical double layers in ionic liquids. This material is available free of charge via the Internet at http://pubs.acs.org.

■ AUTHOR INFORMATION

Corresponding Author

*E-mail: peter.cummings@vanderbilt.edu.

Notes

The authors declare no competing financial interest.

■ ACKNOWLEDGMENTS

This work was supported as part of the Fluid Interface Reactions, Structures and Transport (FIRST) Center, an Energy Frontier Research Center funded by the U.S. Department of Energy, Office of Science, Office of Basic Energy Sciences. The authors acknowledge Dr. Oleg Borodin for graciously providing the APPLE&P force field parameters used in this work. The authors thank the National Energy Research Scientific Computing Center for providing computer time. G.F. appreciates the Palmetto Cluster at Clemson University for providing computer time to complete most simulations performed for this work. V.P. acknowledges funding from the German Federal Ministry for Research and Education (BMBF) in support of the nanoEES^{3D} project (Award No. 03EK3013) as part of the strategic funding initiative energy storage framework. V.P. kindly thanks Prof. Eduard Arzt (INM) for his continuing support.

■ REFERENCES

(1) Conway, B. E. *Electrochemical Supercapacitors: Scientific Fundamentals and Technological Applications*; Kluwer Academic/Plenum Publishers: New York, 1999.

(2) Simon, P.; Gogotsi, Y. Materials for Electrochemical Capacitors. *Nat. Mater.* **2008**, *7*, 845−854.

(3) Itoi, H.; Nishihara, H.; Kogure, T.; Kyotani, T. Three-Dimensionally Arrayed and Mutually Connected 1.2-Nm Nanopores for High-Performance Electric Double Layer Capacitor. *J. Am. Chem. Soc.* **2011**, *133*, 1165−1167.

(4) Korenblit, Y.; Rose, M.; Kockrick, E.; Borchardt, L.; Kvit, A.; Kaskel, S.; Yushin, G. High-Rate Electrochemical Capacitors Based on Ordered Mesoporous Silicon Carbide-Derived Carbon. *ACS Nano* **2010**, *4*, 1337−1344.

(5) Lu, W.; Hartman, R.; Qu, L.; Dai, L. Nanocomposite Electrodes for High-Performance Supercapacitors. *J. Phys. Chem. Lett.* **2011**, *2*, 655−660.

(6) Masarapu, C.; Zeng, H. F.; Hung, K. H.; Wei, B. Effect of Temperature on the Capacitance of Carbon Nanotube Supercapacitors. *ACS Nano* **2009**, *3*, 2199−2206.

(7) Kamat, P. V. Graphene-Based Nanoassemblies for Energy Conversion. *J. Phys. Chem. Lett.* **2011**, *2*, 242−251.

(8) Pech, D.; Brunet, M.; Durou, H.; Huang, P.; Mochalin, V.; Gogotsi, Y.; Taberna, P.-L.; Simon, P. Ultrahigh-Power Micrometre-Sized Supercapacitors Based on Onion-Like Carbon. *Nat. Nanotechnol.* **2010**, *5*, 651−654.

(9) Zhang, L. L.; Zhou, R.; Zhao, X. S. Graphene-Based Materials as Supercapacitor Electrodes. *J. Mater. Chem.* **2010**, *20*, 5983−5992.

(10) Ma, J.; Tang, J.; Zhang, H.; Shinya, N.; Qin, L.-C. Ultrathin Carbon Nanotube Fibrils of High Electrochemical Capacitance. *ACS Nano* **2009**, *3*, 3679−3683.

(11) Izadi-Najafabadi, A.; Futaba, D. N.; Iijima, S.; Hata, K. Ion Diffusion and Electrochemical Capacitance in Aligned and Packed Single-Walled Carbon Nanotubes. *J. Am. Chem. Soc.* **2010**, *132*, 18017−18019.

(12) Ohno, H. *Electrochemical Aspects of Ionic Liquids*; Wiley-Interscience: New York, 2005.

(13) Tsai, W.-Y.; Lin, R.; Murali, S.; Li Zhang, L.; McDonough, J. K.; Ruoff, R. S.; Taberna, P.-L.; Gogotsi, Y.; Simon, P. Outstanding Performance of Activated Graphene Based Supercapacitors in Ionic Liquid Electrolyte from −50 to 80 °C. *Nano Energy* **2013**, http://dx.doi.org/10.1016/j.nanoen.2012.11.006.

(14) Kornyshev, A. A. Double-Layer in Ionic Liquids: Paradigm Change? *J. Phys. Chem. B* **2007**, *111*, 5545−5557.

(15) Lockett, V.; Horne, M.; Sedev, R.; Rodopoulos, T.; Ralston, J. Differential Capacitance of the Double Layer at the Electrode/Ionic Liquids Interface. *Phys. Chem. Chem. Phys.* **2010**, *12*, 12499−12512.

(16) Alam, M. T.; Islam, M. M.; Okajima, T.; Ohsaka, T. Measurements of Differential Capacitance at Mercury/Room-Temperature Ionic Liquids Interfaces. *J. Phys. Chem. C* **2007**, *111*, 18326−18333.

(17) Baldelli, S. Surface Structure at the Ionic Liquid-Electrified Metal Interface. *Acc. Chem. Res.* **2008**, *41*, 421−431.

(18) Trulsson, M.; Algotsson, J.; Forsman, J.; Woodward, C. E. Differential Capacitance of Room Temperature Ionic Liquids: The Role of Dispersion Forces. *J. Phys. Chem. Lett.* **2010**, *1*, 1191−1195.

(19) Feng, G.; Jiang, D.; Cummings, P. T. Curvature Effect on the Capacitance of Electric Double Layers at Ionic Liquid/Onion-Like Carbon Interfaces. *J. Chem. Theory Comput.* **2012**, *8*, 1058−1063.

(20) Shim, Y.; Kim, H. J. Nanoporous Carbon Supercapacitors in an Ionic Liquid: A Computer Simulation Study. *ACS Nano* **2010**, *4*, 2345−2355.

(21) Lin, R.; Taberna, P.-L.; Fantini, S.; Presser, V.; Pérez, C. R.; Malbosc, F.; Rupesinghe, N. L.; Teo, K. B. K.; Gogotsi, Y.; Simon, P. Capacitive Energy Storage from −50 to 100 °C Using an Ionic Liquid Electrolyte. *J. Phys. Chem. Lett.* **2011**, *2*, 2396−2401.

(22) Simon, P.; Gogotsi, Y. Capacitive Energy Storage in Nanostructured Carbon−Electrolyte Systems. *Acc. Chem. Res.* **2012**, DOI: 10.1021/ar200306b.

(23) Huang, J.; Sumpter, B. G.; Meunier, V.; Yushin, G.; Portet, C.; Gogotsi, Y. Curvature Effects in Carbon Nanomaterials: Exohedral Versus Endohedral Supercapacitors. *J. Mater. Res.* **2010**, *25*, 1525−1531.

(24) Lockett, V.; Sedev, R.; Ralston, J.; Horne, M.; Rodopoulos, T. Differential Capacitance of the Electrical Double Layer in Imidazolium-Based Ionic Liquids: Influence of Potential, Cation Size, and Temperature. *J. Phys. Chem. C* **2008**, *112*, 7486−7495.

(25) Silva, F.; Gomes, C.; Figueiredo, M.; Costa, R.; Martins, A.; Pereira, C. M. The Electrical Double Layer at the [BMIM][PF6] Ionic Liquid/Electrode Interface − Effect of Temperature on the Differential Capacitance. *J. Electroanal. Chem.* **2008**, *622*, 153−160.

(26) Holovko, M.; Kapko, V.; Henderson, D.; Boda, D. On the Influence of Ionic Association on the Capacitance of an Electrical Double Layer. *Chem. Phys. Lett.* **2001**, *341*, 363−368.

(27) Vatamanu, J.; Borodin, O.; Smith, G. D. Molecular Insights into the Potential and Temperature Dependences of the Differential Capacitance of a Room-Temperature Ionic Liquid at Graphite Electrodes. *J. Am. Chem. Soc.* **2010**, *132*, 14825−14833.

(28) Boda, D.; Henderson, D.; Chan, K.-Y. Monte Carlo Study of the Capacitance of the Double Layer in a Model Molten Salt. *J. Chem. Phys.* **1999**, *110*, 5346−5350.

(29) Boda, D.; Henderson, D. The Capacitance of the Solvent Primitive Model Double Layer at Low Effective Temperatures. *J. Chem. Phys.* **2000**, *112*, 8934−8938.
(30) Dzyuba, S. V.; Bartsch, R. A. Influence of Structural Variations in 1-Alkyl(Aralkyl)-3-Methylimidazolium Hexafluorophosphates and Bis(Trifluoromethylsulfonyl)Imides on Physical Properties of the Ionic Liquids. *ChemPhysChem* **2002**, *3*, 161−166.
(31) Fredlake, C. P.; Crosthwaite, J. M.; Hert, D. G.; Aki, S. N. V. K.; Brennecke, J. F. Thermophysical Properties of Imidazolium-Based Ionic Liquids. *J. Chem. Eng. Data* **2004**, *49*, 954−964.
(32) Lindahl, E.; Hess, B.; van der Spoel, D. Gromacs 3.0: A Package for Molecular Simulation and Trajectory Analysis. *J. Mol. Model.* **2001**, *7*, 306−317.
(33) Borodin, O. Polarizable Force Field Development and Molecular Dynamics Simulations of Ionic Liquids. *J. Phys. Chem. B* **2009**, *113*, 11463−11478.
(34) Bedrov, D.; Borodin, O.; Li, Z.; Smith, G. D. Influence of Polarization on Structural, Thermodynamic, and Dynamic Properties of Ionic Liquids Obtained from Molecular Dynamics Simulations. *J. Phys. Chem. B* **2010**, *114*, 4984−4997.
(35) Feng, G.; Cummings, P. T. Supercapacitor Capacitance Exhibits Oscillatory Behavior as a Function of Nanopore Size. *J. Phys. Chem. Lett.* **2011**, *2*, 2859−2864.
(36) Feng, G.; Qiao, R.; Huang, J.; Dai, S.; Sumpter, B. G.; Meunier, V. The Importance of Ion Size and Electrode Curvature on Electrical Double Layers in Ionic Liquids. *Phys. Chem. Chem. Phys.* **2011**, *13*, 1152−1161.
(37) Feng, G.; Huang, J.; Sumpter, B. G.; Meunier, V.; Qiao, R. A "Counter-Charge Layer in Generalized Solvents" Framework for Electrical Double Layers in Neat and Hybrid Ionic Liquid Electrolytes. *Phys. Chem. Chem. Phys.* **2011**, *13*, 14723−14734.
(38) Feng, G.; Zhang, J. S.; Qiao, R. Microstructure and Capacitance of the Electrical Double Layers at the Interface of Ionic Liquids and Planar Electrodes. *J. Phys. Chem. C* **2009**, *113*, 4549−4559.
(39) Yeh, I. C.; Berkowitz, M. L. Ewald Summation for Systems with Slab Geometry. *J. Phys. Chem.* **1999**, *111*, 3155−3162.
(40) Hess, B.; Bekker, H.; Berendsen, H. J. C.; Fraaije, J. G. E. M. Lincs: A Linear Constraint Solver for Molecular Simulations. *J. Comput. Chem.* **1997**, *18*, 1463−1472.
(41) Vatamanu, J.; Cao, L.; Borodin, O.; Bedrov, D.; Smith, G. D. On the Influence of Surface Topography on the Electric Double Layer Structure and Differential Capacitance of Graphite/Ionic Liquid Interfaces. *J. Phys. Chem. Lett.* **2011**, *2*, 2267−2272.
(42) Fedorov, M. V.; Kornyshev, A. A. Towards Understanding the Structure and Capacitance of Electrical Double Layer in Ionic Liquids. *Electrochim. Acta* **2008**, *53*, 6835−6840.
(43) Si, X.; Li, S.; Wang, Y.; Ye, S.; Yan, T. Effects of Specific Adsorption on the Differential Capacitance of Imidazolium-Based Ionic Liquid Electrolytes. *ChemPhysChem* **2012**, *13*, 1671−1676.
(44) Bazant, M. Z.; Storey, B. D.; Kornyshev, A. A. Double Layer in Ionic Liquids: Overscreening Versus Crowding. *Phys. Rev. Lett.* **2011**, *106*, 046102.
(45) Georgi, N.; Kornyshev, A. A.; Fedorov, M. V. The Anatomy of the Double Layer and Capacitance in Ionic Liquids with Anisotropic Ions: Electrostriction Vs. Lattice Saturation. *J. Electroanal. Chem.* **2010**, *649*, 261−267.
(46) Largeot, C.; Portet, C.; Chmiola, J.; Taberna, P.-L.; Gogotsi, Y.; Simon, P. Relation between the Ion Size and Pore Size for an Electric Double-Layer Capacitor. *J. Am. Chem. Soc.* **2008**, *130*, 2730−2731.
(47) Kim, T. Y.; Lee, H. W.; Stoller, M.; Dreyer, D. R.; Bielawski, C. W.; Ruoff, R. S.; Suh, K. S. High-Performance Supercapacitors Based on Poly(Ionic Liquid)-Modified Graphene Electrodes. *ACS Nano* **2010**, *5*, 436−442.
(48) Wu, P.; Huang, J.; Meunier, V.; Sumpter, B. G.; Qiao, R. Voltage Dependent Charge Storage Modes and Capacity in Subnanometer Pores. *J. Phys. Chem. Lett.* **2012**, *3*, 1732−1737.
(49) Israelachvili, J. N. *Intermolecular and Surface Forces*; Academic Press: New York, 1992.
(50) Vatamanu, J.; Borodin, O.; Bedrov, D.; Smith, G. D. Molecular Dynamics Simulation Study of the Interfacial Structure and Differential Capacitance of Alkylimidazolium Bis-(Trifluoromethanesulfonyl)Imide [C_nMIM][TFSI] Ionic Liquids at Graphite Electrodes. *J. Phys. Chem. C* **2012**, *116*, 7940−7951.
(51) Li, S.; Feng, G.; Fulvio, P. F.; Hillesheim, P. C.; Liao, C.; Dai, S.; Cummings, P. T. Molecular Dynamics Simulation Study of the Capacitive Performance of a Binary Mixture of Ionic Liquids near an Onion-Like Carbon Electrode. *J. Phys. Chem. Lett.* **2012**, *3*, 2465−2469.
(52) Costa, R.; Pereira, C. M.; Silva, F. Double Layer in Room Temperature Ionic Liquids: Influence of Temperature and Ionic Size on the Differential Capacitance and Electrocapillary Curves. *Phys. Chem. Chem. Phys.* **2010**, *12*, 11125−11132.